The Astrophysical Journal, 670: L73–L76, 2007 December 1

SEARCHING FOR NON-GAUSSIAN SIGNALS IN THE BOOMERANG 2003 CMB MAPS

G. De Troia,[1,2] P. A. R. Ade,[3] J. J. Bock,[4,5] J. R. Bond,[6] J. Borrill,[7,8] A. Boscaleri,[9] P. Cabella,[10] C. R. Contaldi,[6,11] B. P. Crill,[12] P. de Bernardis,[2] G. De Gasperis,[1] A. de Oliveira-Costa,[13] G. Di Stefano,[14] P. G. Ferreira,[10] E. Hivon,[15] A. H. Jaffe,[11] T. S. Kisner,[7,8] M. Kunz,[16] W. C. Jones,[4,5] A. E. Lange,[5] M. Liguori,[17] S. Masi,[2] S. Matarrese,[18] P. D. Mauskopf,[3] C. J. MacTavish,[6] A. Melchiorri,[2,19] T. E. Montroy,[20] P. Natoli,[1,21] C. B. Netterfield,[22] E. Pascale,[22] F. Piacentini,[2,23] D. Pogosyan,[24] G. Polenta,[2] S. Prunet,[15] S. Ricciardi,[2,25] G. Romeo,[14] J. E. Ruhl,[26] P. Santini,[2] M. Tegmark,[13] M. Veneziani,[2,27] and N. Vittorio,[1,21]

Received 2007 May 11; accepted 2007 October 15; published 2007 October 29

ABSTRACT

We analyze the BOOMERANG 2003 (B03) 145 GHz temperature map to constrain the amplitude of a non-Gaussian, primordial contribution to CMB fluctuations. We perform a pixel-space analysis restricted to a portion of the map chosen in view of high-sensitivity, very low foreground contamination and tight control of systematic effects. We set up an estimator based on the three Minkowski functionals which relies on high-quality simulated data, including non-Gaussian CMB maps. We find good agreement with the Gaussian hypothesis and derive the first limits based on BOOMERANG data for the nonlinear coupling parameter $f_{\rm NL}$ as $-300 < f_{\rm NL} < 650$ at 68% CL and $-800 < f_{\rm NL} < 1050$ at 95% CL.

Subject heading: cosmic microwave background

1. INTRODUCTION

While cosmology is entering its precision era, the target of experiments aimed at the cosmic microwave background (CMB) is shifting toward weak signals, e.g., polarization, the SZ effect, and non-Gaussian (NG) features. Detection of NG signals can be of significant help in constraining the mechanisms that explain the generation of cosmological perturbations. Provided that systematic effects will not degrade high-sensitivity CMB mapping, present and future experiments could in principle be sensitive to nonlinearities due to second-order effects in perturbation theory (Bartolo et al. 2004). This signal is usually parameterized by a nonlinear coupling factor $f_{\rm NL}$ that controls the level of a quadratic contribution to the primordial gravitational potential Φ (Komatsu & Spergel 2001):

$$\Phi(\boldsymbol{x}) = \Phi_{\rm G}(\boldsymbol{x}) + f_{\rm NL}[\Phi_{\rm G}(\boldsymbol{x})^2 - \langle \Phi_{\rm G}(\boldsymbol{x})^2 \rangle], \quad (1)$$

where $\Phi_{\rm G}$ is a zero-mean, Gaussian random field.

Several groups have reported NG constraints on CMB data. All suborbital efforts to date have found no significant deviation from Gaussianity in the CMB field: MAXIMA-1 reported $|f_{\rm NL}| < 950$ at 1 σ (Santos et al. 2003; Wu et al. 2001), while the Very Small Array found an upper limit of 5400 at 2 σ (Smith et al. 2004); the Archeops group have recently improved their limits to $-800 < f_{\rm NL} < 1100$ (2 σ), although their analysis is based on assumptions only valid for the large angular scales dominated by the Sachs-Wolfe effect (Curto et al. 2007). The BOOMERANG 1998 data set has also been tested for Gaussianity, both in pixel (Polenta et al. 2002) and in Fourier (De Troia et al. 2003) space, finding no trace of NG signals. However, BOOMERANG has set no $f_{\rm NL}$ limit so far. One of the purposes of this Letter is to provide such limits with the analysis of the new 2003 (B03) data. The limits presented here are more stringent than those found by any suborbital experiment to date, properly accounting for subhorizon angular scales.

The *WMAP* team constrained $f_{\rm NL}$ to be $-54 < f_{\rm NL} < 114$ (Spergel et al. 2006). Using an improved version of the *WMAP* team estimator, Creminelli et al. (2007) set the most stringent limits to date at $-36 < f_{\rm NL} < 100$. Thus the $f_{\rm NL}$ analysis does not show any departure from Gaussianity in *WMAP* data. However, some authors have looked at general deviations from Gaussianity (i.e., not based on any specific parameterization of NG) and claimed highly significant detection of NG features in the *WMAP* maps (Copi et al. 2004; Vielva et al. 2004; Cruz et al. 2006).

In this Letter we perform a pixel-space analysis of the B03 temperature (T) data set, using the observed field's moments and Minkowski functionals (MFs) to build Gaussianity tests. We assess the statistical significance of our results by com-

[1] Dipartimento di Fisica, Università Tor Vergata, Roma, Italy.
[2] Dipartimento di Fisica, Università La Sapienza, Roma, Italy.
[3] Department of Physics and Astronomy, Cardiff University, Cardiff CF24 3YB, Wales, UK.
[4] Jet Propulsion Laboratory, Pasadena, CA.
[5] Observational Cosmology, California Institute of Technology, Pasadena, CA.
[6] Canadian Institute for Theoretical Astrophysics, University of Toronto, Toronto, ON, Canada.
[7] Computational Research Division, Lawrence Berkeley National Laboratory, Berkeley, CA.
[8] Space Sciences Laboratory, University of California, Berkeley, CA.
[9] IFAC-CNR, Firenze, Italy.
[10] Astrophysics, University of Oxford, Keble Road, Oxford OX1 3RH, UK.
[11] Theoretical Physics Group, Imperial College, London, UK.
[12] IPAC, California Institute of Technology, Pasadena, CA.
[13] Department of Physics, Massachusetts Institute of Technology, Cambridge, MA.
[14] Istituto Nazionale di Geofisicae Vulcanologia, Roma, Italy.
[15] Institut d'Astrophysique, Paris, France.
[16] Département de Physique Théorique, Université de Genève, Switzerland.
[17] Department of Applied Mathematics and Theoretical Physics, University of Cambridge, UK.
[18] Dipartimento di Fisica G. Galilei, Università di Padova and INFN, Sezione di Padova, Italy.
[19] INFN, Sezione di Roma 1, Roma, Italy.
[20] Sierra Lobo, Inc., 11401 Hoover Road, Milan, OH 44846.
[21] INFN, Sezione di Tor Vergata, Roma, Italy.
[22] Physics Department, University of Toronto, Toronto, ON.
[23] European Space Astronomy Centre (ESAC), European Space Agency, Madrid, Spain.
[24] Department of Physics, University of Alberta, Edmonton, AB, Canada.
[25] INAF–Osservatorio Astronomico di Padova, Italy.
[26] Physics Department, Case Western Reserve University, Cleveland, OH.
[27] APC, 10 rue Alice Domon et Léonie Duquet, 75205 Paris Cedex 13, France.

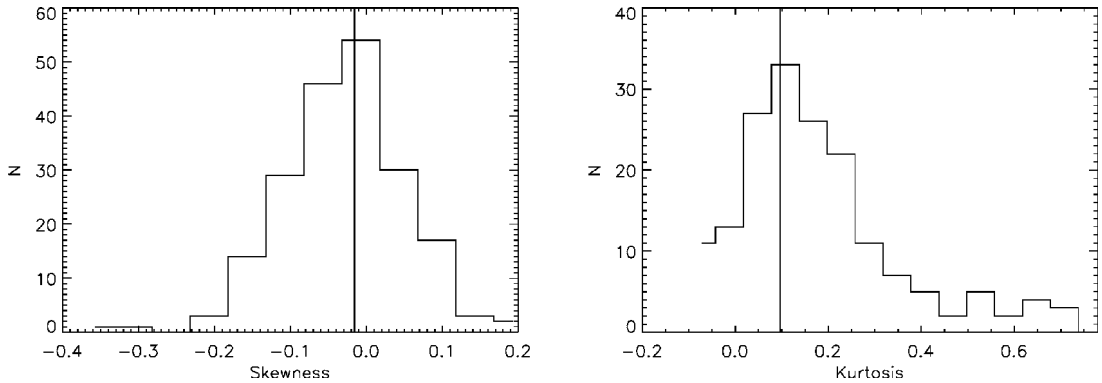

FIG. 1.—*Left*: Distribution of S_3 estimator calculated from the 200 Gaussian MC maps. The S_3 value of the B03 data is represented by the vertical line. *Right*: Same, for S_4.

paring the data to a set of highly realistic, Gaussian Monte Carlo (MC) simulated maps. In order to constrain $f_{\rm NL}$, we build a goodness-of-fit statistics based on MFs and calibrated against a set of NG CMB maps that are generated according to the algorithm set forth in Liguori et al. (2003).

The plan of this Letter is as follows: in § 2 we briefly describe the B03 experiment, the data set it has produced, and our simulation pipeline. In § 3 we compute the map's moments and MFs of the data and compare results against Gaussian MC simulated maps. Then we derive constraints for $f_{\rm NL}$. Finally, in § 4 we draw our main conclusions.

2. THE BOOMERANG 2003 DATA SET

The balloon-borne B03 experiment was flown from Antarctica in 2003. It gathered data for 14 days in three frequency bands, centered at 145, 245, and 345 GHz. Here we restrict ourselves to the 145 GHz data, which are most sensitive to CMB fluctuations. These have been obtained with polarization-sensitive bolometers (PSBs). The analysis of the data set has produced high-quality maps of the southern sky that have been conveniently divided in three regions: a "deep" (in terms of integration time) survey region (∼90 deg^2) and a "shallow" survey region (∼750 deg^2), both at high Galactic latitudes, as well as a region of ∼300 deg^2 across the Galactic plane. The deep region is completely embedded in the shallow region. Here we only consider a subset of the data that contains all of the deep region and part of the shallow, for a total of 693 deg^2 (1.7% of the sky). The mask we use is square, 26° on a side, centered at about R.A. = 82.6° and decl. = −44.2°, and excludes all detected point sources in the field. This region has been selected in view of high-sensitivity CMB observation with low foreground contamination and was observed with a highly connected scanning strategy to keep systematics under control. We use the T data map reduced jointly from eight PSBs at 145 GHz (Masi et al. 2006). In this region, the signal rms on 3.4′ pixels is ∼90 μK and instrumental noise has an rms of ∼20 μK in the deep region and ∼90 μK in the shallow region. In harmonic space, binned estimates of the CMB angular power spectrum retain signal-to-noise ratios >1 well beyond $l \sim 1000$. One may compare these figures with *WMAP*: in the 3 year release, the *WMAP* combined sensitivity in the region observed by B03 is ∼100 μK on 3.4′ pixels, close to *WMAP*'s mean pixel error. However, *WMAP*'s beams are broader than B03, so its l-space error is ∼5 times larger than B03 at $l \simeq 1000$. On the other hand, B03 was not devised to measure multipoles at $l \lesssim 50$. In this sense, our NG analysis probes angular scales complementary to those constrained by *WMAP*. While we do not consider here the Stokes Q and U polarization maps, our T map has been marginalized with respect to linear polarization. For a description of the instrument and the measured T and polarization maps, see Masi et al. (2006), and for the CMB TT, TE, and EE power spectra, see Jones et al. (2006), Piacentini et al. (2006), and Montroy et al. (2006).

To assess the robustness of our tests of Gaussianity we use a set of simulated MC maps that mimic the B03 data. To produce these, we follow the same steps performed when analyzing real data. The Gaussian CMB sky signal is simulated from the power spectra that best fit the B03 data (MacTavish et al. 2006). This signal is smoothed according to the measured beam and synthesized into a pixelized sky map, using HEALPix routines (Górski et al. 2005). Using the B03 scanning strategy, the signal map is projected onto eight time streams, one for each 145 GHz detector. Noise-only time streams are also produced, as Gaussian realizations of each detector's noise power spectral density, which are estimated from the data accounting for cross talk among detectors. The time lines are reduced with the ROMA map-making code (Natoli et al. 2001; de Gasperis et al. 2005) replicating the actual flight pointing and transient flagging, to produce T, Q, and U maps. With this procedure, we can simulate signal, noise, and signal plus noise time stream.

To constrain $f_{\rm NL}$ we use MC simulations of NG CMB maps obtained from a primordial gravitational potential of the form given in equation (1). These maps have been produced including first-order CMB radiative transfer effects (Liguori et al. 2003). The power spectrum of the NG maps is identical to that of the Gaussian CMB simulations.

3. TESTS OF GAUSSIANITY AND CONSTRAINTS ON $f_{\rm NL}$

Working at 6.8′ HEALPix resolution ($N_{\rm side} = 512$), we first compute the normalized skewness S_3 and kurtosis S_4 of our pixelized field T_i. These are obtained from the variance $\sigma^2 = 1/(N-1)\sum_i (T_i - \langle T\rangle)^2$ and from the third and the fourth moments $\mu_3 = \sum_i (T_i - \langle T\rangle)^3/N$ and $\mu_4 = \sum_i (T_i - \langle T\rangle)^4/N$, where N is the total number of pixels of the map and $\langle T\rangle = \sum_i T_i/N$ its mean. We have $S_3 = \mu_3/\sigma^3$, $S_4 = \mu_4/\sigma^4 - 3$. From the data we get $S_3 = -0.016$ and $S_4 = 0.096$. These values are plotted in Figure 1 as a vertical line and compared to the empirical distribution as derived from the MC (signal plus noise) maps. From the latter we compute the probabilities $P(S_3^{\rm sim} > S_3^{\rm data}) = 58\%$ and $P(S_4^{\rm sim} > S_4^{\rm data}) = 77\%$. Hence, for these tests the data are compatible with the Gaussian hypothesis. The same tests are repeated after having degraded the map to 13.6′, finding similar results.

To analyze the map with MFs (Gott et al. 1990), we consider

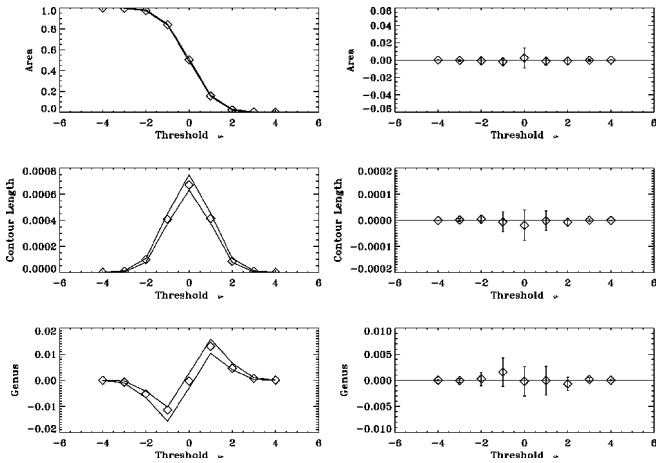

FIG. 2.—*Left*: MFs estimated from the B03 data (*diamonds*) and the 2 σ confidence limits from the 200 Gaussian MC maps. From top to bottom, the results correspond to the MFs M0, M1, and M2, respectively. *Right*: Residuals between the MC mean and the data.

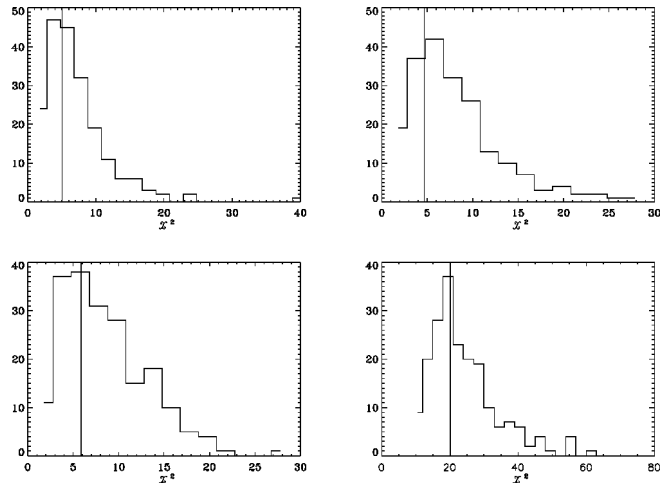

FIG. 3.—The χ^2_B distribution (*histogram*) of MC simulated maps and data value (*vertical line*) for the MFs. *Top*: Area (*left*) and contour length (*right*). *Bottom*: Genus (*left*) and "joint" estimator (*right*; see text).

the excursion sets Q defined as the map's subsets exceeding a given threshold ν: $Q(\nu) = \{T_i : (T_i - \langle T\rangle)/\sigma > \nu\}$. The three MFs measure the total area of the surviving regions of the map (M_0), their total contour length (M_1), and the genus of the distribution, which is related to the difference between the number of "hot" and "cold" regions (M_2). For a Gaussian field the expectation values of the functionals depend on a single parameter τ: $\langle M_0(\nu)\rangle = \frac{1}{2}[1 - \mathrm{erf}(\nu/\sqrt{2})]$, $\langle M_1(\nu)\rangle = (\sqrt{\tau}/8)\exp(-\nu^2/2)$, $\langle M_2(\nu)\rangle = [\tau/(8\pi^3)^{1/2}]\nu\exp(-\nu^2/2)$. In the case of a pure CMB signal (no noise), τ is given by $\tau = \frac{1}{2}\sum_{l=1}^{\infty}(2l+1)\,l(l+1)C_l$ (Schmalzing & Górski 1998; Winitzki & Kosowsky 1998). Hence, M_1 and M_2 depend on the power spectrum C_l. It is hence critical that the simulations reproduce the model C_l's that best fit the data. We work in the flat-sky limit, projecting our T values on the plane locally tangent to the map (Cabella et al. 2004). In Figure 2 we plot MFs for the data and 2 σ limits set by 200 Gaussian simulations, as well as the data residuals and their (again, 2 σ) errors. The functionals are computed at nine thresholds evenly spaced between -4 σ and $+4$ σ.

Using the MC maps we can define a χ^2 statistic:

$$\chi^2_{B,i} = \sum_{\nu\nu'}(M_i^B - \langle M_i^{\rm sim}\rangle)_\nu C^{-1}_{i,\nu\nu'}(M_i^B - \langle M_i^{\rm sim}\rangle)_{\nu'}. \qquad (2)$$

Here M_i^B ($M_i^{\rm sim}$) is any of the three MFs obtained from the data (simulations), $\langle\cdots\rangle$ is the mean value over MC realizations, and $C_{i,\nu\nu'} = \langle(M_{i,\nu} - \langle M_{i,\nu}\rangle)(M_{i,\nu'} - \langle M_{i,\nu'}\rangle)\rangle$ is a covariance matrix, estimated from an independent set of ~1000 Gaussian maps. In the top left, top right, and bottom left panels of Figure 3 we show χ^2_i for each MF (*vertical line*), plotted along with the empirical distribution sampled via MC. We can define a "joint" estimator by grouping the M_i's in a single, 27 element data vector $M_J \equiv \{M_0, M_1, M_2\}$ and defining a χ^2_B as a trivial extension of equation (2). It is important that the covariance matrix built for the joint estimator correctly account for correlations among different functionals. However, we have found that in order to pin down to a stable level these off-block couplings, one requires a number realizations significantly higher than the ~1000 used throughout our analysis. The latter number cannot be realistically increased to desired level, because the GLS map-making procedure is a demanding computational task, even for the supercomputers we have used. Fortunately, we have found that using white (instead of correlated) noise to estimate the covariance matrix has a negligible impact on the analysis. This finding can indeed be justified a posteriori, because the GLS map-making procedure is very effective in suppressing noise correlations, which contribute very weakly to the estimator's final covariance. The joint χ^2 of the data is displayed as the bottom right panel in Figure 3, along with the MC empirical distribution. The probability $P(\chi^2 > \chi^2_B)$ that a Gaussian map has a larger χ^2 than the B03 map is 76% for M_0, 83% for M_1, 76% for M_2, and 67% for the "joint" estimator. The values are fully consistent with the Gaussian hypothesis. We conclude that our pixel-space analysis does not detect any sign of NG behavior in the B03 data.

We now want to constrain the quadratic coupling parameter $f_{\rm NL}$ defined in equation (1). To this purpose we simulate NG CMB realizations in the following way: first, we generate the Gaussian and NG part of the primordial potential defined by equation (1); then we convolve them with CMB first-order radiation transfer functions to get the final CMB sky. In this way we produce 200 **G** (Gaussian) maps and 200 **NG** counterparts (each **G** map has a uniquely defined **NG** counterpart), so that for a given $f_{\rm NL}$ our (signal only) map is $\mathbf{G} + f_{\rm NL} * \mathbf{NG}$. By adding noise maps, we can define the MF estimators as discussed above, with the difference that they are now functions of $f_{\rm NL}$: $J_B(f_{\rm NL}) = M_J^B - \langle M_J(f_{\rm NL})\rangle$ (we only consider the "joint" estimator in what follows). Consequently, we now define the data χ^2 as $\chi^2_B(f_{\rm NL}) = J_B(f_{\rm NL})^T\mathbf{C}^{-1}J_B(f_{\rm NL})$. While in principle the covariance of the M_J's is a function of $f_{\rm NL}$, this dependence is expected to be weak and is usually neglected (Komatsu et al. 2003). We have tested for this explicitly by using our NG simulations. We plot χ^2_B as a function of $f_{\rm NL}$ in Figure 4 (*left panel*). Goodness-of-fit analysis yields $-300 < f_{\rm NL} < 650$ at 68% CL and $-800 < f_{\rm NL} < 1050$ at 95%, with a best-fit value (χ^2_B at its minimum) of $f_{\rm NL} = 200$. In order to cross-check this result, we estimate a "frequentist" confidence interval for $f_{\rm NL}$ by sampling the empirical distribution of the M_J-based χ^2, computed for $f_{\rm NL} = 200$. The resulting histogram is displayed in the right panel of Figure 4. This analysis shows that we should expect to constrain $|f_{\rm NL}| \lesssim 1000$ at 95%, thus suggesting that our limits derived through goodness-of-fit analysis are consistent. One may consider what limits on $f_{\rm NL}$ would be derived if we use, in place of MFs, the map's skewness and kurtosis defined above as elements of a two-dimensional data vector. We thus repeated our goodness-of-fit analysis using

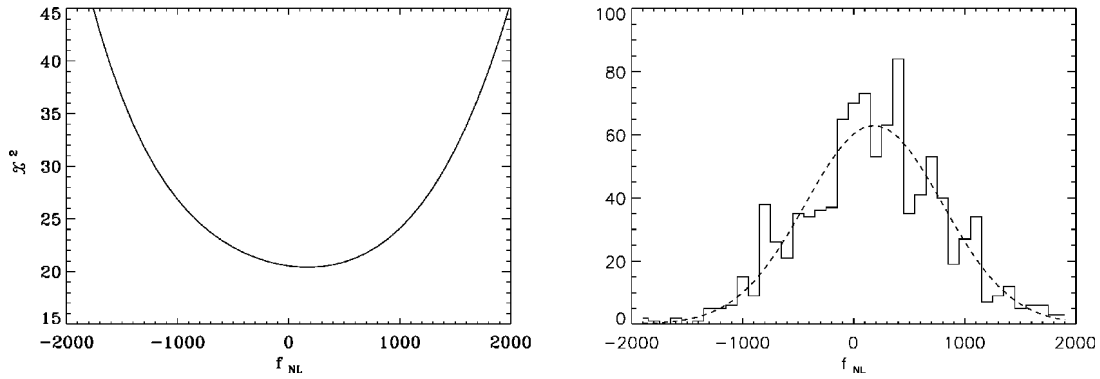

FIG. 4.—*Left*: B03 data χ^2 (χ^2_B in the text) as a function of $f_{\rm NL}$. *Right*: Empirical χ^2 distribution for NG maps ($f_{\rm NL} = 200$), sampled using 1000 simulations

these statistics and found weaker limits: $-950 < f_{\rm NL} < 1350$ at 68% CL ($-1400 < f_{\rm NL} < 1800$ at 95% CL). Even so, it is quite remarkable that a crude one-point pixel statistic degrades the final sensitivity only by a factor ~2. Of course, in order to find "optimal" constraints one has to implement a more sophisticated analysis.

The B03 data set is not expected to be noise dominated at the 6.8′ resolution employed in the analysis above. To show that this is the case, we repeated all of our procedures for 13.6′, finding similar (although slightly weaker) constraints.

4. CONCLUSIONS

We analyzed the B03 145 GHz T map in search of NG signals. We worked in pixel space at 6.8′ and 13.6′ HEALPix resolution. We computed the skewness and kurtosis of the map, as well as its three MFs. We compared these estimates against a set of simulated Gaussian maps that have been reduced using the same analysis pipeline as real data, finding no evidence of NG behavior. To quantify the latter statement, we define goodness-of-fit statistics jointly based on all three MFs, showing that the probability for a Gaussian simulation to have a χ^2 larger than the data is ~67%. Assuming a model for primordial fluctuations that predicts a quadratic perturbation to the gravitational potential, we set limits on the nonlinear coupling parameter $f_{\rm NL}$ as $-800 < f_{\rm NL} < 1050$ at 95% CL ($-300 < f_{\rm NL} < 650$ at 68% CL). These limits may be regarded as complementary to the constraints set by *WMAP* in view of the better signal-to-noise ratio at high resolution in the B03 field.

BOOMERANG was supported by CIAR, CSA, and NERSC in Canada, ASI, University La Sapienza and PNRA in Italy, and NASA and NSF in the US. We thank CASPUR and NERSC/LBL. We acknowledge the use of HEALPix.

REFERENCES

Bartolo, N., Komatsu, E., Matarrese, S., & Riotto, A. 2004, Phys. Rep., 402, 103
Cabella, P., et al. 2004, Phys. Rev. D, 69, 063007
Copi, C. J., Huterer, D., & Starkman, G. D. 2004, Phys. Rev. D, 70, 043515
Creminelli, P., et al. 2007, J. Cosmol. Astropart. Phys., 3, 5
Cruz, M., et al. 2006, MNRAS, 369, 57
Curto, A., et al. 2007, A&A, 474, 23
de Gasperis, G., et al. 2005, A&A, 436, 1159
De Troia, G., et. al. 2003, MNRAS, 343, 284
Górski, K. M., et al. 2005, ApJ, 622, 759
Gott, J. R., et al. 1990, ApJ, 352, 1
Jones, W. C., et. al. 2006, ApJ, 647, 823
Komatsu, E., & Spergel, D. N. 2001, Phys. Rev. D, 63, 063002
Komatsu, E., et al. 2003, ApJS, 148, 119
Liguori, M., Matarrese, S., & Moscardini, L. 2003, ApJ, 597, 57
MacTavish, C. J., et al. 2006, ApJ, 647, 799
Masi, S., et al. 2006, A&A, 458, 687
Montroy, T. E., et al. 2006, ApJ, 647, 813
Natoli, P., et al. 2001, A&A, 372, 346
Piacentini, F., et al. 2006, ApJ, 647, 833
Polenta, G., et. al. 2002, ApJ, 572, L27
Santos, M. G., et al. 2003, MNRAS, 341, 623
Schmalzing, J., & Górski, K. M. 1998, MNRAS, 297, 355
Smith, S., et al. 2004, MNRAS, 352, 887
Spergel, D. N., et al. 2007, ApJS, 170, 377
Vielva, P., et al. 2004, ApJ, 609, 22
Winitzki, S., & Kosowsky, A. 1998, NewA, 3, 75
Wu, J. H. P., et al. 2001, Phys. Rev. Lett., 87, 251303